DOI 10.1007/s11182-023-02847-x
*Russian Physics Journal, Vol. 65, No. 11, March, 2023 (Russian Original No. 11, November, 2022)*

# MAGNETIZATION AND CURIE POINT OF LiZn FERRITE SYNTHESIZED BY ELECTRON BEAM HEATING OF MECHANICALLY ACTIVATED REAGENTS

**E. N. Lysenko, V. A. Vlasov, A. P. Surzhikov, and S. A. Ghyngazov** UDC 621.355

*The paper studies magnetization of* $Li_{0.4}Fe_{2.4}Zn_{0.2}O_4$ *lithium-zinc ferrite sintered by electron beam heating of a mechanically activated mixture of initial* $Fe_2O_3$–$Li_2CO_3$–ZnO *reagents based on measurements of the specific saturation magnetization and Curie point. Initial reagents are mechanically activated in a planetary ball mill for different time at 1290 and 2220 rpm grinding rate. Specimens are heated by using the pulse accelerator ILU-6 at the electron energy of 2.4 MeV. The synthesis temperature is 600 and 750°C at the exposure time not over 120 minutes. It is shown that preliminary grinding at 2220 rpm and successive electron beam heating at 750°C for 120 minutes, lead to the formation of the main ferrite concentration with the chemical formula specified during the reagent mixing. This is confirmed by the data on the specific saturation magnetization of 80 emu/g and the nominal value of the Curie point of 500°C. This mode allows to significantly reduce the ferrite synthesis temperature compared to the traditional ceramic technology.*

**Keywords:** lithium-zinc ferrite, magnetization, Curie point, mechanical activation, electron beam.

## INTRODUCTION

Lithium-zinc (LiZn) ferrite materials possess the high saturation magnetization, Curie point, permeability, and low coercitive force [1−4]. In this regard, lithium-zinc ferrite is widely used in high-frequency electronic devices such as microwave circulators, phase shifters, radar absorbers, and also in computer industry [5−8].

Depending on the morphology of synthesized particles, the following synthesis methods are currently used: solid-phase synthesis, sol-gel technology, microwave heating, etc. [9−14]. As for the LiZn ferrite fabrication, the solid-phase synthesis is based on the high-temperature heating of compacted materials in commercial furnaces using initial $Fe_2O_3$–$Li_2CO_3$–ZnO oxides [15−18]. The main weakness of this technique, is irreproducibility of electromagnetic properties of materials synthesized at high temperatures and, consequently, the stoichiometry violation caused by zinc and lithium evaporation during the synthesis as well as a multi-stage and prolonged production process.

In [19−22], the method of heating the initial oxide mixture is proposed to decrease the temperature and time of the ferrite synthesis comprising readily volatile components using a high-energy electron beam. In the literature, this method is often known as the radiation-thermal synthesis, which provides the electron beam energy over 1 MeV to heat bulk specimens due to the energy interaction and absorption in a solid. Using thermostatically controlled cells, it is possible to gain a uniform depth temperature distribution during the synthesis process [23]. The decrease in the synthesis temperature and duration, is gained *via* the higher rate of the solid phase interaction between initial oxides due to the radiation defect formation by the electron beam [24−27]. The inclusion of the preliminary compaction procedure in the production process, allows to enhance the fabrication of lithium ferrites, especially in the case of lithium-substituted ferrites with complex compositions [28].

National Research Tomsk Polytechnic University, Tomsk, Russia, e-mail: lysenkoen@tpu.ru; vlvitan@tpu.ru; surzhikov@tpu.ru; ghyngazov@tpu.ru. Translated from Izvestiya Vysshikh Uchebnykh Zavedenii, Fizika, No. 11, pp. 86–92, November, 2022. Original article submitted October 12, 2022; accepted for publication October 20, 2022.

 

TABLE 1. Process Parameters and Specimen Abbreviations

| Specimens | Modes | Mechanical activation, rpm | Synthesis temperature, °C |
|---|---|---|---|
| MA1_T_600 | Thermal synthesis | 1290 | 600 |
| MA1_T_750 | Thermal synthesis | 1290 | 750 |
| MA2_T_600 | Thermal synthesis | 2220 | 600 |
| MA2_T_750 | Thermal synthesis | 2220 | 750 |
| T_600 | Thermal synthesis | – | 600 |
| T_750 | Thermal synthesis | – | 750 |
| MA1_RT_600* | Radiation-thermal synthesis | 1290 | 600 |
| MA1_ RT_750 | Radiation-thermal synthesis | 1290 | 750 |
| MA2_ RT_600 | Radiation-thermal synthesis | 2220 | 600 |
| MA2_ RT_750 | Radiation-thermal synthesis | 2220 | 750 |
| RT_600 | Radiation-thermal synthesis | – | 600 |
| RT_750 | Radiation-thermal synthesis | – | 750 |

*RT – radiation-thermal synthesis.

In [29−31], it was demonstrated that the rate of the solid phase interaction during the ferrite synthesis, was increased *via* the preliminary mechanical activation of initial powders in a ball mill. This procedure combined with the electron beam heating provided the synthesis of ferrite powders without the preliminary compaction of materials [32].

The aim of this work is to study the magnetic properties of lithium-zinc ferrite material synthesized by using the electron beam heating of the mechanically activated mixture of initial $Fe_2O_3$–$Li_2CO_3$–ZnO reagents.

## EXPERIMENTAL

The synthesis of the lithium-zinc (LiZn) ferrite ($Li_{0.4}Fe_{2.4}Zn_{0.2}O_4$) material was based on initial 86.05 wt.% $Fe_2O_3$, 6.64 wt.% $Li_2CO_3$, and 7.31 wt.% ZnO oxides, which were dried and then mixed with each other.

The mechanical activation of the $Fe_2O_3$–$Li_2CO_3$–ZnO powder mixture was performed during 10, 20, 30, 60 and 120 min in a planetary ball mill AGO-2S (OOO, "Novitz" Russia) with steel balls and glasses. Grinding was conducted in a translatory glass motion at 1290 and 2220 rpm rotational velocity.

The synthesis of the LiZn ferrite material utilized the electron beam heating with a pulse accelerator ILU-6 from the Budker Institute of Nuclear Physics SB RAS (Russia) [33]. The operating parameters of the ILU-6 included 2.4 MeV electron beam energy, 400 mA pulse current, 500 μs pulse time. The synthesis temperature ranged between 600 and 750°C and provided by the pulse frequency varying within 5 and 12.5 Hz. The process time did not exceed 120 min.

The obtained results were compared to those obtained for specimens synthesized by the conventional ceramic technology based on the specimen heating in a laboratory furnace under the same temperature-time conditions. The process parameters and specimen abbreviations are given in Table 1.

The specific saturation magnetization was measured by an induction magnetometer N–04 at magnetizing field of 4.7 kOe. The LiZn ferrite material was characterized by the low coercitive force on the order of 1 Oe. It was therefore easily magnetized in the external magnetic field prior to the saturation magnetization. The N–04 was calibrated on a reference specimen.

The Curie point of specimens was detected using the thermomagnetometric analysis based on the thermogravimetric analysis with the applied external magnetic field. The thermal analyzer Netzsch STA 449 C Jupiter® (Germany) and permanent magnets providing the external magnetic field of 4.7 kOe, were used for the measurement of thermal effects. This procedure was described in detail in [34−37].

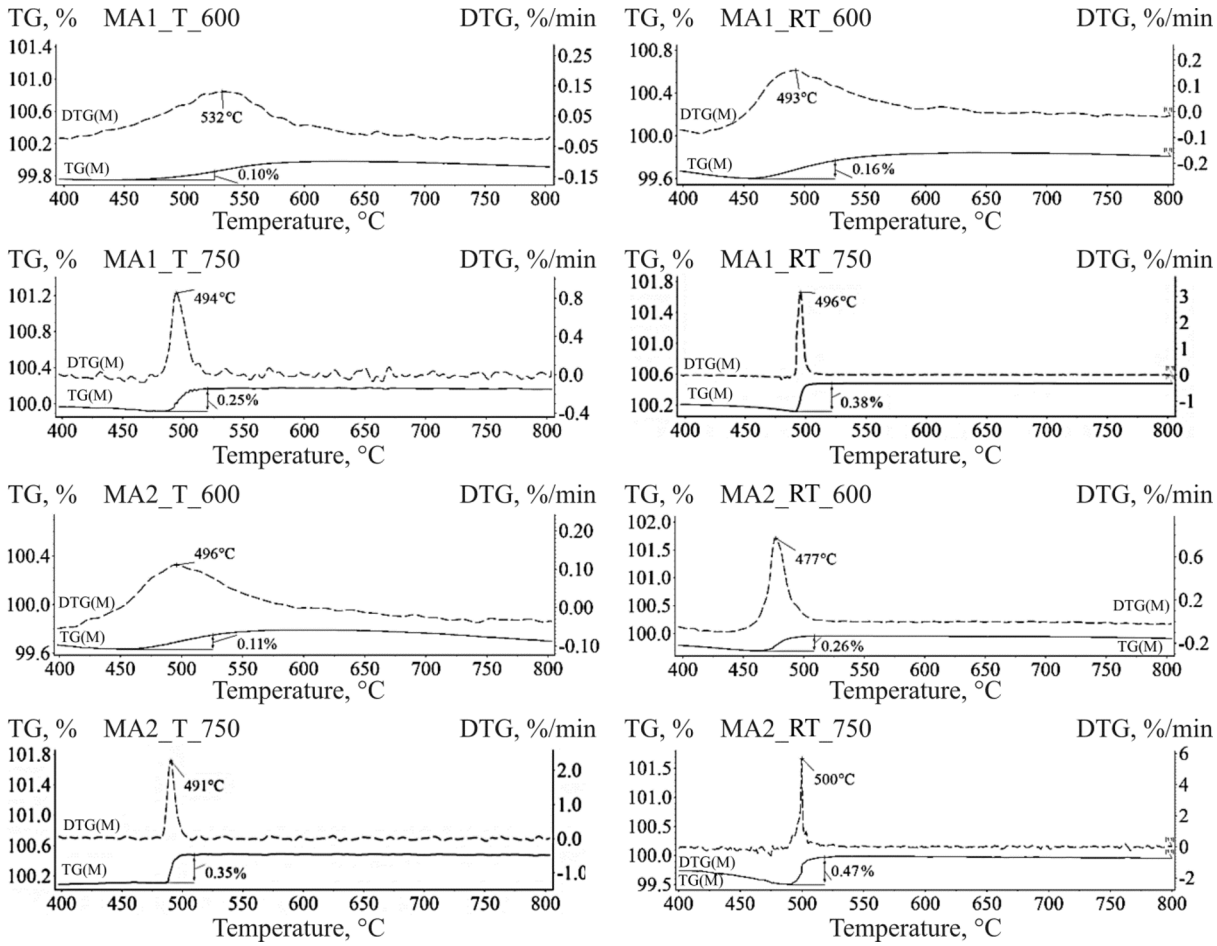


Fig. 1. Thermomagnetometric analysis of LiZn ferrite specimens synthesized during 120 min from mechanically activated powder mixture.

## RESULTS AND DISCUSSION

It is known that, the LiZn ferrite synthesis occurs in accordance with the following formula:

$$Li_2CO_3 + (5-x)(1-x)^{-1}Fe_2O_3 + 4x(1-x)^{-1}ZnO \rightarrow 4(1-x)^{-1}Li_{0.5(1-x)}Fe_{2.5-0.5x}Zn_xO_4 + CO_2.$$

The formation of high permeability ferrite with the $Li_{0.4}Fe_{2.4}Zn_{0.2}O_4$ composition occurs during the synthesis at $x = 0.2$. It is characterized by a spontaneous magnetization and rectangular hysteresis loop.

Figure 1 plots thermogravimetric (TG) and differential thermogravimetric (DTG) curves obtained in specimen heating with the applied external magnetic field. The weight change observed on the TG curve, is associated with the jump in the region of the magnetic phase transition, i.e., the magnetic-to-paramagnetic transition in the synthesized magnetic phase, but it is not associated with the change in the specimen weight. The weight jump value depends on the ferrite phase content and magnetization. The higher its concentration and magnetization, the more intensive is the weight jump. As can be seen in Fig. 1, the weight jump in specimens grows with increasing synthesis temperature, glass rotational velocity, and during the transition from thermal to radiation-thermal synthesis. This indicates to the higher content of the synthesized ferrite phase in these specimens.

The DTG(M) peak position allows us to identify the Curie point of the obtained magnetic phase, whereas its width shows the degree of homogeneity of the ferrite phase composition synthesized in different modes. Wide and

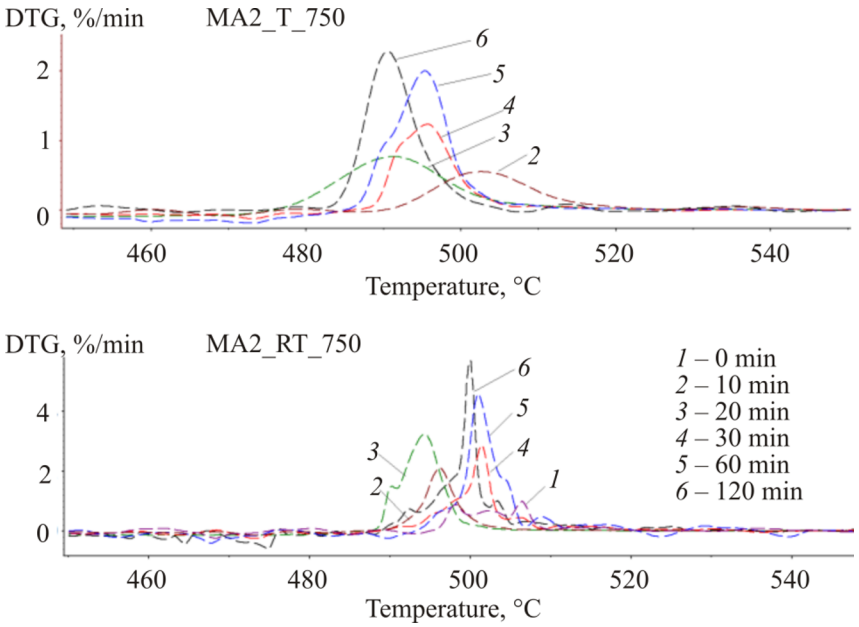


Fig. 2. Thermomagnetometric analysis of LiZn ferrite specimens synthesized at 750°C and different process time.

extended peaks on DTG(M) curves as well as small weight jumps on TG(M) curves observed for MA1_T_600, MA2_T_600, MA1_RT_600 specimens, indicate to the formation of a low concentration of the magnetic phase in the given modes.

According to the thermomagnetometric analysis, the LiZn ferrite content is higher after its synthesis from mechanically activated powders at the Curie point approaching to that of $Li_{0.4}Fe_{2.4}Zn_{0.2}O_4$. At the same time, in our recent research [28], we report on the high content of the intermediate LiZn ferrite phase $Li_{0.5(1-x)}Fe_{2.5-0.5x}Zn_xO_4$ synthesized at different Curie points from non-activated reagents.

The significant LiZn phase accumulation is observed in specimens synthesized at 750°C and different process time. As presented in Fig. 2, the DTG(M) peak intensity means the high content of this phase in specimens produced during 60 min and longer. A comparison of these peak positions by the Curie point of LiZn ferrite to those observed by Abu-Elsaad *et al*. [38], shows that during the electron beam heating at 750°C synthesis for 120 min, the formation of the main ferrite ($Li_{0.4}Fe_{2.4}Zn_{0.2}O_4$) content occurs during the reagent mixing.

Kinetic dependences in Fig. 3 show the equipment weight change ($\Delta H_{TG}$) and the DTG(M) peak height ($\Delta H_{DTG}$) during the thermal analysis of specimens obtained at different synthesis modes. According to the kinetic analysis, at 60-min process time, $\Delta H_{TG}$ curves describing the obtained phase magnetization, get to plateau, that indicates to inexpediency of loner sintering processes. The higher magnetization is observed for specimens synthesized from powders mechanically activated at a higher grinding rate.

Kinetic dependences in Fig. 4 show the specific saturation magnetization of LiZn ferrite specimens obtained at different synthesis modes. The specific saturation magnetization $\sigma_S$ of all specimens, grows with increasing process time, which is associated with the magnetic phase accumulation in these specimens. At short process times, the specific saturation magnetization rapidly grows. During further synthesis, the rate of the change in the specific saturation magnetization drastically slows down, and the curves get to plateau.

Our results show that the temperature growth up to 750°C and the higher grinding rate, accelerate the formation of the magnetic ferrite phase. The electron beam heating of specimens provides them with the high specific saturation magnetization by the beginning of isothermal synthesis (see Fig. 4, reference point of curves). This probably indicates to the high LiZn ferrite concentration, which appears at the stage of specimen heating. The specific saturation magnetization of $Li_{0.4}Fe_{2.4}Zn_{0.2}O_4$ ferrite is close to the nominal value [39, 40].

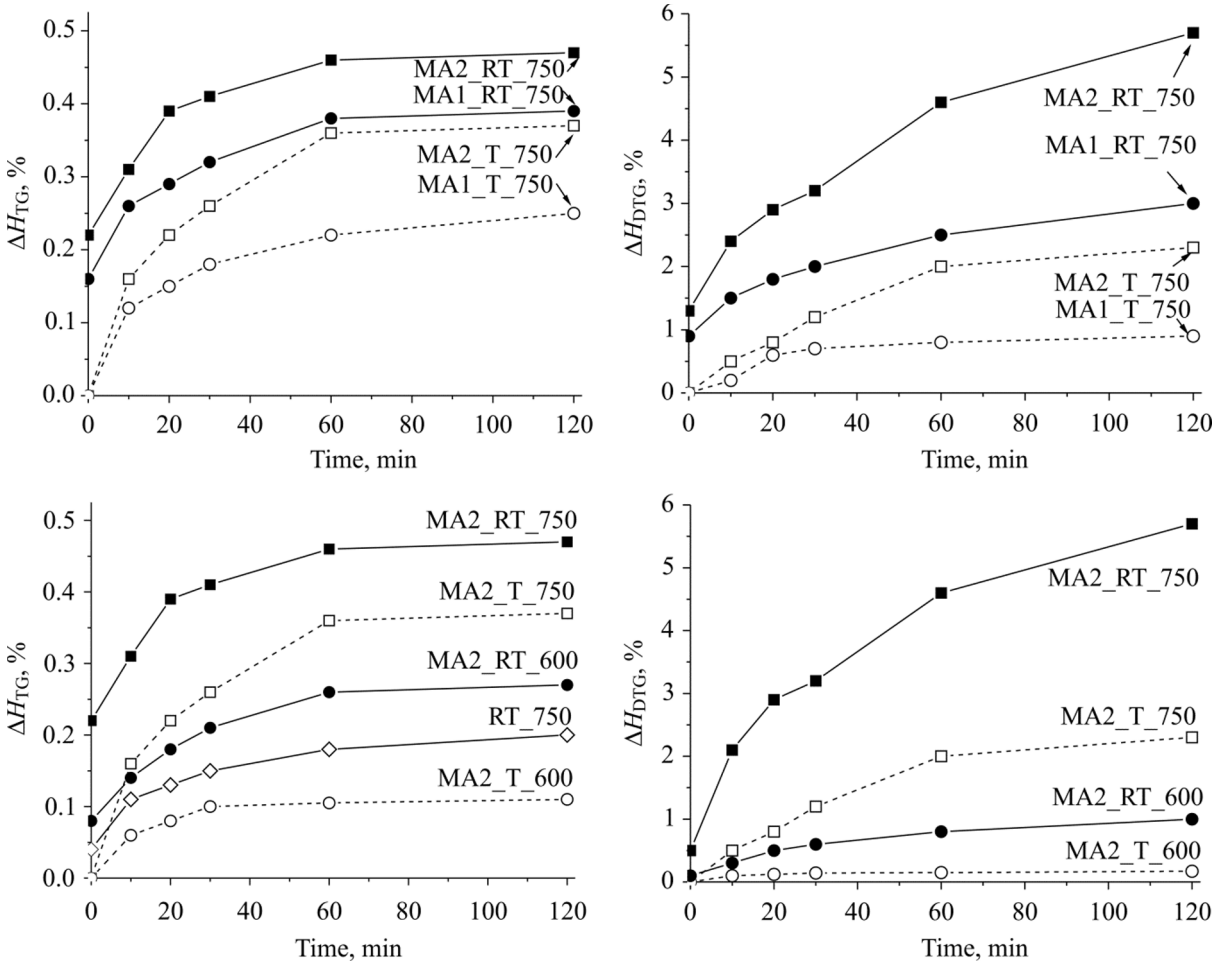


Fig. 3. Kinetic dependences of equipment weight change $\Delta H_{TG}$ and DTG(M) peak height $\Delta H_{DTG}$ during heating LiZn ferrite specimens obtained at different synthesis modes.

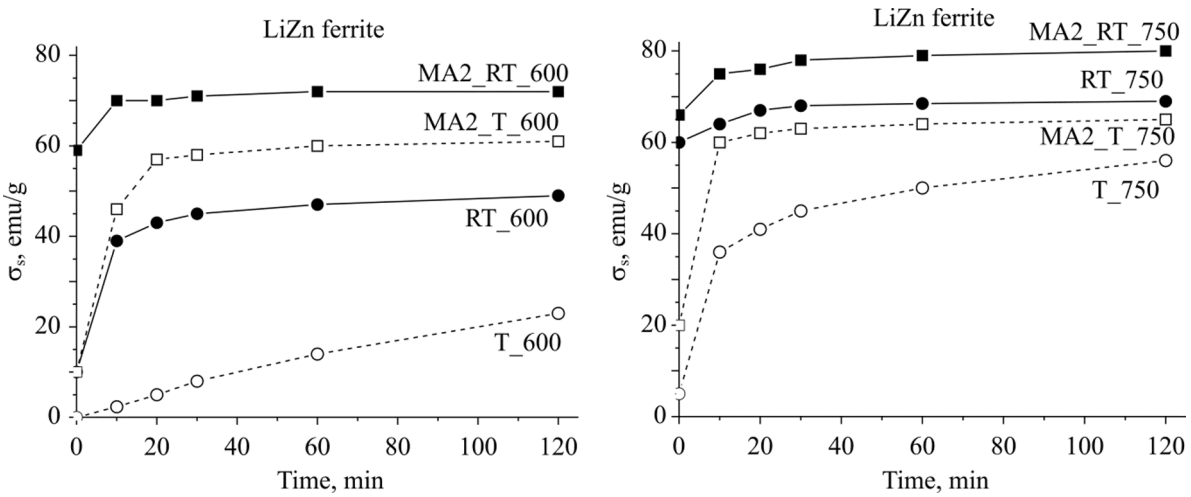


Fig. 4. Kinetic dependences of specific saturation magnetization of LiZn ferrite specimens obtained at different synthesis modes.

The measurement of ferrite magnetic properties showed the accelerated formation of the homogeneous composition of the ferrite phase based on the preliminary mechanical activation of initial reagents followed by the high energy electron beam heating.

## CONCLUSIONS

The specific saturation magnetization and the Curie point were investigated for LiZn ferrite comprising $Li_{0.4}Fe_{2.4}Zn_{0.2}O_4$ synthesized by the electron beam heating of the mechanically activated mixture of initial $Fe_2O_3$–$Li_2CO_3$–ZnO reagents. The analysis of the obtained results showed that the ferrite phase content in synthesized specimens depended on the heating temperature, mechanical activation conditions, and synthesis modes.

In mechanically activated initial powders, the ferrite synthesis was more rapid, that was confirmed by the high values of the specific saturation magnetization and nominal values of the Curie point. The rate of powder grinding in the planetary mill played an important part in the degree of the mechanical activation and, consequently, the number of products synthesized.

Our experiments showed that the high-energy grinding of initial powders and their successive electron beam heating led to the formation of the homogeneous composition of the ferrite phase during the synthesis process. The synthesis temperature of 750°C was significantly lower than 900°C used in the traditional ceramic technology. This fact can exert a positive effect on the ferrite stoichiometric composition also comprising readily volatile components.

## ACKNOWLEDGEMENT

The authors thank M. V. Korobeinikov and A. A. Bryazgin from the Budker Institute of Nuclear Physics SB RAS, Novosibirsk, Russia, for kindly providing the pulse accelerator ILU-6 employed in these studies.

This work was financially supported by Grant No. 22-19-00183 from the Russian Science Foundation.

## REFERENCES

1. A. V. Anupama, V. Rathod, V. M. Jali, and B. Sahoo, J. Alloys Compd., **728**, 1091–1100 (2017). DOI: 10.1016/j.jallcom.2017.09.099.
2. M. S. Ruiz and S. E. Jacobo, Physica B, **407**, 3274–3277 (2012). DOI: 10.1016/j.physb.2011.12.085.
3. Y. Gao and Z. Wang, JMMM, **528**, 167808 (2021). DOI: 10.1016/j.jmmm.2021.167808.
4. M. Mahmoudi and M. Kavanlouei, JMMM, **384**, 276–283 (2015). DOI: 10.1016/j.jmmm.2015.02.053.
5. I. M. Isaev, V. G. Kostishin, V. V. Korovushkin, *et al*., Tech. Phys., **66**, 1216–1220 (2021). DOI: 10.1134/S1063784221090085.
6. Y. Guo, J. Zhu, and H. Li, Ceram. Int., **47**, 9111–9117 (2021). DOI: 10.1016/j.ceramint.2020.12.034.
7. M. H. Al-Dharob, I. M. Abdulmajeed, A. H. Taha, *et al*., Digest J. Nanomater. Biostruct., **17**, No. 1, 201–208 (2022), https://chalcogen.ro/201_Al-DharobMH.pdf.
8. X. Wang, K. Yin, T. Cao, *et al*., J. Alloys Compd., **885**, 160983 (2021). DOI: 10.1016/j.jallcom.2021.160983.
9. G. C. Wakde, V. R. Raghorte, G. B. Pethe, *et al*., Ferroelectrics, **587**, No. 1, 18–32 (2022). DOI: 10.1080/00150193.2022.2034409.
10. D. V. Wagner, O. A. Dotsenko, and V. A. Zhuravlev, Russ. Phys. J., **62**, No. 4, 581–588 (2019).
11. G. R. Gajula, L. R. Buddiga, K. N. Chidambara Kumar, *et al*., J. Sci.: Adv. Mater. Dev., **3**, No. 2, 230–235 (2018). DOI: 10.1016/j.jsamd.2018.04.007.
12. S. Kotru, R. Paul, and A. Q. Jaber, Mater. Chem. Phys., **276**, 125357 (2022). DOI: 10.1016/j.matchemphys.2021.125357.
13. Q. Khan, A. Majeed, N. Ahmad, *et al*., Mater. Chem. Phys., **273**, 125028 (2021). DOI: 10.1016/j.matchemphys.2021.125028.

14. V. A. Zhuravlev, A. V. Zhuravlev, V. V. Atamasov, and G. I. Malenko, Russ. Phys. J., **62**, No. 10, 1926–1936 (2020). DOI: 10.17223/00213411/62/10/162.
15. A. A. Sattar, H. M. El-Sayed, W. R. Agami, and A. A. Ghani, Am. J. Appl. Sci., **4**, No. 2, 89–93 (2007). DOI: 10.3844/AJASSP.2007.89.93.
16. P. Kumar, J. K. Juneja, S. Singh, *et al*., Ceram. Int., **41**, 3293–3297 (2015). DOI: 10.1016/j.ceramint.2014.10.092.
17. P. Kumar, J. K. Juneja, C. Prakash, *et al*., Ceram. Int., **40**, 2501–2504 (2014). DOI: 10.1016/j.ceramint.2013.07.063.
18. L. Jia, Y. Zhao, F. Xie, *et al*., AIP Adv., **6**, 056214 (2016). DOI: 10.1063/1.4943928.
19. V. G. Kostishin, R. I. Shakirzyanov, A. G. Nalogin, *et al*., Phys. Solid State, **63**, No. 3, 435–441 (2021). DOI: 10.1134/S1063783421030094.
20. V. G. Kostishin, V. G. Andreev, V. V. Korovushkin, *et al*., Inorg. Mater., **50**, 1317 (2014). DOI: 10.1134/S0020168514110089.
21. V. G. Kostishin, V. V. Korovushkin, A. G. Nalogin, *et al*., Phys. Solid State, **62**, 1156 (2020). DOI: 10.1134/S1063783420070124.
22. V. A. Zhuravlev, E. P. Naiden, R. V. Minin, *et al*., IOP Conf. Ser.: Mater. Sci. Eng., **81**, 012003 (2015). DOI: 10.1088/1757-899X/81/1/012003.
23. E. N. Lysenko, E. V. Nikolaev, V. A. Vlasov, and A. P. Surzhikov, Nucl. Instrum. Methods Phys. Res. B, **474**, 49–56 (2020). DOI: 10.1016/j.nimb.2020.04.026.
24. V. L. Auslender, I. G. Bochkarev, V. V. Boldyrev, *et al*., Solid State Ion., **101–103**, 489–493 (1997).
25. N. Z. Lyakhov, V. V. Boldyrev, A. P. Voronin, *et al*., J. Therm. Anal. Calorim., **43**, 21−31 (1995). DOI: 10.1007/BF02635965.
26. V. V. Boldyrev, A. P. Voronin, O. S. Gribkov, *et al*., Solid State Ion., **36**, 1–6 (1989). DOI: 10.1016/0167-2738(89)90051-9.
27. E. N. Lysenko, A. P. Surzhikov, A. V. Malyshev, *et al*., Izv. Vyssh. Uchebn. Zaved., Khimiya i khimicheskaya tekhnologiya, **61**, No. 6, 69–75 (2018).
28. E. N. Lysenko, V. A. Vlasov, A. P. Surzhikov, and A. I. Kupchishin, Inorg. Mater.: Appl. Res., **13**, No. 2, 494–500 (2022).
29. S. A. Mazen and N. I. Abu-Elsaad, JMMM, **442**, 72–79 (2017).
30. V. Berbenni, A. Marini, P. Matteazzi, *et al*., J. Eur. Ceram. Soc., **23**, 527–536 (2003). DOI: 10.1016/S0955-2219(02)00150-4.
31. A. P. Surzhikov, E. N. Lysenko, A. V. Malyshev, and O. G. Vasil'eva, Izv. Vyssh. Uchebn. Zaved., Fiz., **56**, No. 1/2, 159–162 (2013).
32. E. N. Lysenko, V. A. Vlasov, and A. P. Surzhikov, Nucl. Nucl. Instrum. Methods Phys. Res. B, **466**, 31–36 (2020). DOI: 10.1016/j.nimb.2020.01.010.
33. V. L. Auslender, A. A. Bryazgin, B. L. Faktorovich, *et al*., J. Radiat. Phys. Chem., **63**, 613–615 (2002). DOI: 10.1016/S0969-806X(01)00672-7.
34. A. L. Astafyev, E. N. Lysenko, and A. P. Surzhikov, J. Therm. Anal. Calorim., **136**, 441–445 (2019).
35. D. M. Lin, H. S. Wang, M. L. Lin, *et al*., J. Therm. Anal. Calorim., **58**, 347–353 (1999). DOI: 10.1023/A:1010199004211.
36. P. K. Gallagher, J. Therm. Anal. Calorim., **49**, 33–44 (1997). DOI: 10.1007/BF01987419.
37. M. E. Brown and P. K. Gallagher, eds., Handbook of Thermal Analysis and Calorimetry, Vol. 5, Elsevier Science (2008). DOI: 10.1016/S1573-4374(13)60004-7.
38. N. I. Abu-Elsaad, S. A. Mazen, and H. M. Salem, J. Alloys Compd., **835**, 155227 (2020). DOI: 10.1016/j.jallcom.2020.155227.
39. P. V. B. Reddy, V. R. Reddy, A. Gupta, *et al*., Hyperfine Interaction, **183**, 81–86 (2008).
40. P. V. B. Reddy, B. Ramesh, and C. G. Reddy, Physica B, **405**, 1852–1856 (2010). DOI: 10.1016/j.physb.2010.01.062.